PROCEEDINGS OF SCIENCE

A search for gamma-ray emission from a sample of magnetized white dwarfs using Fermi-LAT data.

Spencer. T. Madzime[a,*] **and P.J. Meintjes**[a]

[a] *Department of Physics, University of the Free State,*
205 Nelson Mandela Dr, Park West, Bloemfontein, South Africa

E-mail: tsmadzime@gmail.com, MeintjPJ@ufs.ac.za

We present the preliminary results for the search of gamma-ray emission from three magnetized white dwarfs (EUVE J0317-855, CTCV J2056-3014, LAMOST J024048.51+195226.9) using the Fermi-LAT pass 8 dataset. This search is influenced by the recent indications of possible pulsed gamma-ray from AE Aquarii and AR Scorpii using Fermi-LAT data. A search for gamma-ray emission from these sources were conducted using a ∼ 14-year baseline of the archived upgraded Fermi-LAT pass 8 dataset. For all of these sources a standard unbinned and binned analyses have been performed, resulting in no significant gamma-ray excess above the background noise at the location of each source. However, flagging data with TS > 0 showing good convergence using the likelihood analysis, as well as data sections with TS > 4 (for comparison), resulted in evidence of sporadic gamma-ray emission that could be distinguished above the background emission. This can be considered somewhat analogous to phase gating, i.e. flagging events not associated with the main pulse of a pulsar's pulsed emission to search for weak emitters in its immediate vicinity. Gamma-ray emissions modulated at the spin period of each white dwarf were searched for using the Rayleigh test for sparse data. Pulsed emission has been detected at the spin-period of all three sources, i.e. EUVE J0317-855 (P_* = 724.673 s; $-\log$ Prob = 4.823), CTCV J2056-3014 (P_* = 29.6 s; $-\log$ Prob = −7.51), LAMOST J024048.51+195226.9 (P_* = 24.93 s; $-\log$ Prob = 5.796). To produce a phase-folded light curve the pulse arrival times were folded with an ephemeris, specified in the text. The overall statistical significance for all three sources appears to be ∼ 5 σ after taking into account statistical penalties based on a duty cycle of ∼ 30% due to the data flagging we introduced.

High Energy Astrophysics in Southern Africa 2022 - HEASA2022
28 September - 1 October 2022
Brandfort, South Africa

*Speaker

PoS(HEASA2022)055

1. Introduction

White dwarfs are compact objects composed of degenerate matter, which can not undergo any further nuclear fusion. Usually lower-mass stars in the mass range $0.8 \leq M_{\odot} \leq 8$ end-up as white dwarfs e.g., [1–3]. These progenitor stars can either be solitary stars or be in a wide binary system. It is probable that the formation of solitary white dwarfs with substantial magnetic fields and rapid rotation are linked to the interaction of closely orbiting binary star systems e.g., [4, 5]. Highly magnetized white dwarfs are believed to originate from two different mechanisms e.g., [6–8]: The first is through mergers, where the collision and combination of two white dwarfs can create a fast rotating magnetized white dwarf if the newly formed object rotates rapidly and has a high magnetic field. The second mechanism involves dynamo processes that occur within the white dwarf's interior, which convert the kinetic energy from rotation into magnetic energy and lead to the formation of a powerful magnetosphere. Rapid rotation and a strong magnetic field are the main ingredients of particle acceleration in the vicinity of compact objects in general e.g., [9–15].

The theoretical studies of rapidly rotating and highly magnetized white dwarfs revealed that these compact objects can accelerate particles to higher energies in order of tera electron Volt (TeV), e.g. [9–15]. Thus, rapidly rotating and magnetized white dwarfs are likely to produce soft gamma-rays mimicking the same process as believed to occur in magnetars, soft gamma-ray repeaters (SGRs) and anomalous X-ray pulsars (AXPs) [16–19]. Magnetars are solitary neutron stars powered by magnetic energy. For an in-depth understanding of rotation powered white dwarfs refer to Meintjes et al [9]. These authors show that curvature radiation of relativistic electrons close to the surface of the white dwarf may play a very important role to produce gamma-rays with energies below $\epsilon_{\gamma} \leq 50\,\mathrm{GeV}$.

The recent indication of possible transient low level gamma-ray emission from AE Aquarii [20–22] and AR Scorpii [23] in Fermi LAT data motivated this study. Thus, 3 non-accreting rapidly rotating magnetized white dwarfs have been selected for this study (e.g., EUVE J0317-855, CTCV J2056-3014, and LAMOST J024048.51+195226.9). This contribution paper is structured as follows : In the following section is a brief overview of the sources considered for this study will be presented. Fermi-LAT data acquisition and analysis are discussed next, followed by the presentation of the preliminary results for each source. Lastly, a discussion and conclusions section will be presented.

2. Properties of Three Magnetic White Dwarfs Selected for this Study

2.1 EUVE J0317 - 855

EUVE J0317 - 855 (J0317) is a highly magnetized white dwarf with dipole field strength of 350 MG [24]. J0317 is an extreme-ultraviolet (EUV) source (EUVE, and ROSAT e.g, [24]). The photometric and wavelength-averaged circular polarization data show variations at 725 s periodicity [24, 25]. J0317 exhibits a strongly structured circular polarization spectrum (8 % peak polarization, [25]). Ferrario et al. [25] pointed out that the polarization and optical photometric variations can be explained by the oblique rotator model. J0317 maybe the end product of a double-degenerate merger inferring from its properties i.e. high mass, high rotational rate, and age discrepancy with a close white dwarf companion [25].

2.2 CTCV J2056−3014

CTCV J2056−301 (J2056) is a fast (29.6 s, [26]) rotating magnetic CV with an orbital period of 1.76 hours [27]. It is a nearby source at a distance of 261±7.4 pc [28]. J2056 was first presumed to be an intermediate polar (IP, [27, 29]) following the detection of a 15.4 min periodicity in the optical photometry data, and the detection of a relatively bright X-ray counterpart in the ROSAT (PSPC) Bright Source Catalog. The results of follow-up optical spectroscopy conducted by Oliveira et al. [30] show that J2056's spectrum is consistent with spectral features in unusual IPs with short orbital periods i.e., Hβ, Hα and He 4686 emission. J2056 is highly variable with visual magnitude varying between M_V ~17.6 and 15.2 mag (e.g., [27, 28]). This system also display strong flickering with maximum amplitude reaching 0.8 mag.

2.3 LAMOST J024048.51+195226.9

LAMOST J024048.51+195226.9 (J024048) is a magnetic CV [31] with a rapidly rotating white dwarf (period of 24.93 s) [32]. The M1.5(±1) dwarf and the white dwarf are orbiting the common center of mass with a period of 7.3364376 hours [33, 34]. It is considered a possible twin of AE Aquarii (Thorstensen 2020). The detection of pulsations modulated at the spin period of the white dwarf in J024048 establishes it as another white dwarf magnetic propeller system, after AE Aquarii. Garnavich et al. [35] observed that during flares the Balmer emission lines broadened up to ±3000 km/s, and confirmed the presence of a P Cygni-like component in Hα [36], which they also show was consistent with a magnetic propeller model proposed by Wynn et al. [37]. Radio emission were first detected by Pretorius et al. [38], with luminosity 2.7± 3×10^{-17} erg s^{-1} Hz^{-1} (L-band centred at 1284 MHz), which is higher than that of AE Aquarii and close to the highest measured luminosities of any CV.

3. Observation & Analysis of Fermi-LAT data

Fermi-LAT gamma-ray photons collected from the start of the Fermi mission up to 2022-03-25 at 05:21:17 were considered. The 14-year dataset was analysed using the Fermi Science Tools software packages (v11r0p5). The latest response function (P8R3_SOURCE_V2_v1) was used in the analysis and corresponding source-class events (evclass=128) and FRONT+BACK event type (evtype=3) were used to select events within 10 degrees region of interest (ROI) centred at source of interest. This radius is chosen to accommodate the point spread function (PSF) of the LAT instrument (e.g., [39, 40]). To prevent photon contamination by photons produced from cosmic-ray interaction with the atmosphere, the zenith angle cut was set at 90 degrees. Binned maximum likelihood [41] analysis was performed on the energy range 0.1-500 GeV using gtlike, pyLikelihood, and fermipy to validate consistency of results. The statistical significance ($\sigma = \sqrt{TS}$), with $TS = -2\left(L_{\max,\circ}/L_{\max,1}\right)$. Here $L_{\max,\circ}$ and $L_{\max,1}$ represent the maximum likelihood without and with an extra source at the given location being investigated [41]. The significance σ is the level at which the null-hypothesis, i.e. no excess gamma-ray emission from the region of interest (ROI), can be rejected.

"TS-gating" was employed to enhance the visibility of a weak point source within the bright background. This is akin to phase gating, a method utilized for the detection of faint sources in

close proximity to bright pulsars. Phase gating involves [42, 43] selecting the pulsar's off peak phase sections of the data to search for weak emission signatures associated with the pulsar, or weak sources in the immediate vicinity. On the other hand for the so-called "TS-gating" we select segments of data associated with light curve that exhibited model convergence for the binned likelihood analysis. The selected sections corresponded to light curve bins that displayed model convergence with likelihood test statistics greater than zero (TS > 0). This was then followed selecting data sections which show convergence for TS > 4 for comparison. It's important to note that this technique exclude all light curve bins with negative test statistics. For this study, the light curve was generated using an unbinned likelihood analysis approach, which treats each event individually. The duty cycle of the TS-gated data for analysis is about $\alpha \sim 0.3$, which will be implemented as a statistical penalty when the significance of the emission is evaluated for all three sources. For our particular analysis, where data sections have been selected based on limiting TS-values, we adapted the standard methodology by estimating the significance using both the TS-gated and the ungated data (which will represent the noise)

$$\sigma \approx 0.3 \times \sqrt{[\sum_{0.1\,GeV}^{50\,GeV}(TS(\text{gated histogram})) - \sum_{0.1\,GeV}^{50\,GeV}(TS(\text{ungated histrogram}))]} \qquad (1)$$

where we utilized an energy range between 0.1 GeV $\leq \epsilon_\gamma \leq$ 50 GeV. However, it will be showed that the energy bins above 10 GeV contributed very little to the overall emission and hence we restricted our search for periodicity to the energy range between 0.5 GeV $\leq \epsilon_\gamma \leq$ 10 GeV.

Potential pulsed gamma-ray emission was investigated in the Fermi-LAT gamma-ray data, to affirm our results measured using binned likelihood analysis. We employed the Rayleigh test for sparse data commonly used in gamma-ray astronomy when no a priori information of the light curve shape is known [44] and Fermi plug-in [45], which uses the TEMPO2 [46] radio timing analysis tool. Fermi-LAT photon events within the energy range of 0.5-10 GeV, extracted from ROI with a radius of 0.6° around each source of interest were considered. We followed the Fermi-LAT (*gtselect* and *gmktime*) event selection process to select all events associated with the source of interest. Employing *gtpsearch* routine of the Fermi tools (version 10) the photons events were initially folded using the Rayleigh folding analysis algorithm and the ephemeris. In addition, the data was phased using the peak period from *gtpsearch*, and the appropriate ephemeris utilizing the Fermi plug-in. For each source a control analysis was performed on off-source data where we performed the same analysis on data 2°, 4° and 6° away from the source. This was to evaluate whether any periodic modulation was unique to the source's position in the sky. The Fermi science tools (version 10) gtpsearch routine, as well as tempo2 and the Fermi plugin, have built-in functions for conducting barycentric correction. As a result, we supplied the required parameters (e.g., source position and the spacecraft file) for the correction to be carried out.

4. Results

The binned analysis performed on EUVE J0317-855, CTCV J2056-3014, and LAMOST J024048.51+195226.9 resulted in the maximum likelihood test statistic less than the detection level of Fermi-LAT. Therefore, the TS-gating technique was used to produce the energy flux spectrum

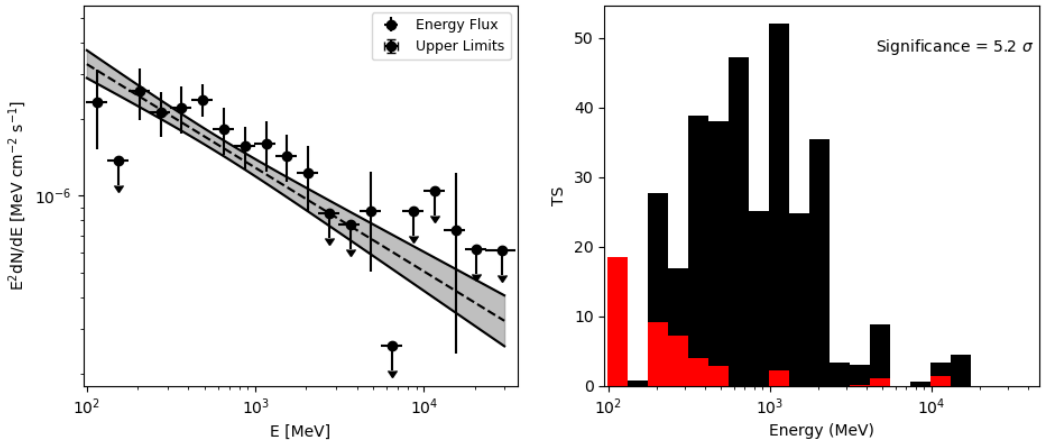

Figure 1: The energy flux spectrum plot of EUVE J0317 - 855 over the energy range 0.1−500 GeV for the entire observation period is displayed with a power-law model fitted to the energy flux points with a photon index 1.8 ± 0.92. Left panel: is generated through binned analysis from events selected using TS gating briefly discussed earlier; Right panel: The corresponding significance of the TS-gated data (Black) and ungated (noise) data (Red) distributed as a function of energy for each energy bin with measurable signal, which reveals a significance of (5.2 σ) using Equation 1 with the emission restricted mainly to lower energy bins $\epsilon_\gamma \leq 10\,\mathrm{GeV}$.

points, counts maps and test statistics (TS) map presented in this manuscript. Observed Counts map showcases the observed counts of gamma-ray sources within the region of interest (ROI). The model predicted counts map presents the predicted counts generated by the model. Significant sources included in the model display their respective predicted counts (Npred). The counts residual map reveals the disparity between predicted counts and observed counts. It serves as an indicator of the model's accuracy, highlighting locations where significant discrepancies exist between predicted and observed counts. Extreme negative or positive counts at specific locations signify overestimated or underestimated counts, respectively. Lastly the model predicted for all sources in the field, excluding the source of interest, have been removed to reveal the statistical significance of the emission of the source of interest's position in the field [41].

The Rayleigh test was used to search for periodicity utilizing the full data baseline of 14 years for all three sources. For comparison off-source data was selected 2°, 4° and 6° away from the source to evaluate whether possible pulsed emission was associated mainly with the position of the source in the sky. The results for each source will be discussed separately.

4.1 EUVE J0317 - 855

EUVE J0317-855 was detected with a relative significance level of 5.2 σ based on the TS-gated dataset, and it exhibited a predicted count of 1664 with an energy flux of $(2.746\times10^{-6}\pm2.04\times10^{-7}$ MeV cm^{-2} s^{-1}). The Fermi-LAT energy flux spectrum of EUVE J0317-855 displays a power-law model with an index of 1.8 ± 0.92, as presented in Figure 1. Figure 2 displays vital maps based on the TS-gated dataset which suggests a gamma-ray excess from EUVE J0317 - 855: (a) the observed counts map, (b) the model predicted counts, (c) the counts residual map and where (d) presents the TS residual map, highlighting excess gamma-rays at the location of EUVE J0317 - 855. These

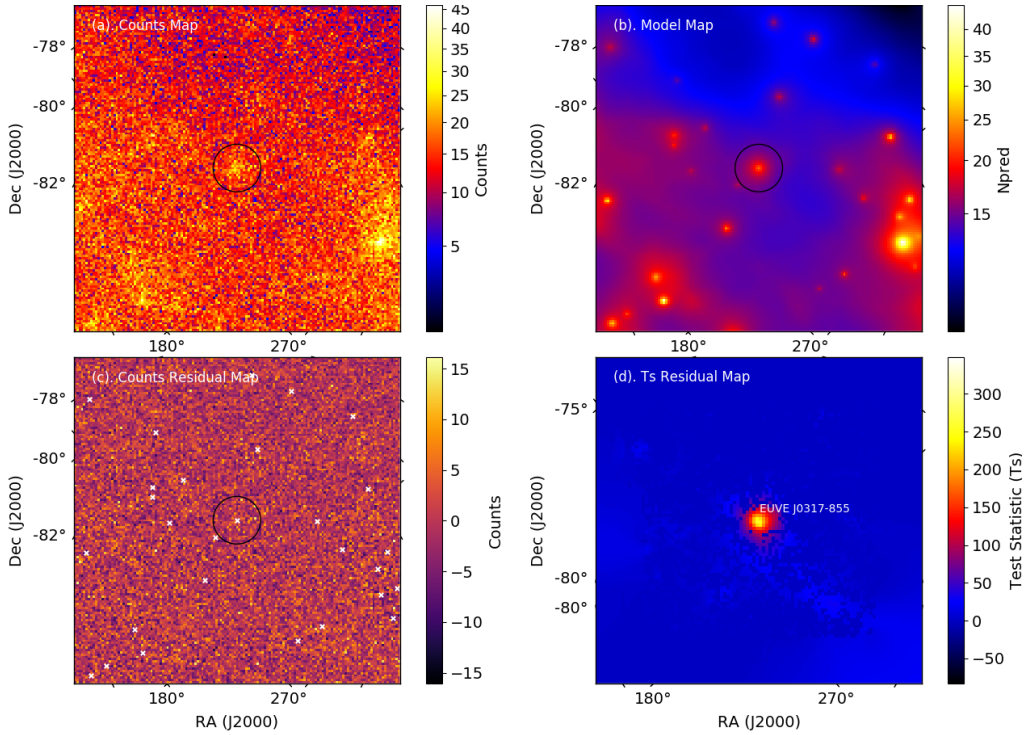

Figure 2: (a) Observed counts map, (b) model predicted counts map, (c) the counts residual map. All significant sources included in the model will show with their predicted counts (Npred). The residual map displays the goodness of the model. If there is a huge difference between predicted counts and observed counts the effect will be seen as extreme negative or positive counts at the location where counts are overestimated or underestimated. (d) TS residual map shows excess γ-rays above the background at the location of EUVE J0317 - 855 at the 5.2 σ significance level when the model predictions for the rest of the sources in the field have been removed.

maps collectively assess the model's accuracy e.g., by comparing observed and predicted counts. We searched for periodic oscillations in the energy range with energy maximum set at 10 GeV using photon events within 0.6° ROI. We used the pulsed ephemeris T_0 = 2450237.715035 BJD derived from Ferrario et al. [25] to assign phases to the photon events. The phased light curve and the Rayleigh test power spectrum are presented in Figure 3.

Our control analysis in the off-source regions (Figure 4) seems to suggest that the pulsations seem to have lost most of its coherence outside the Fermi-LAT 4° window which tentatively seems to suggest that the periodic emission is restricted to the position of the source in the sky.

4.2 CTCV J2056−3014

CTCV J2056−3014 was detected with a relative significance level exceeding 4.9 σ using the TS-gated dataset, and it exhibited a predicted count of 1912 with an energy flux of $(1.66 \times 10^{-6} \pm 1.52 \times 10^{-7}$ MeV cm^{-2} s^{-1}). The Fermi-LAT energy flux of CTCV J2056−3014 displays a power-law spectrum with an index of 2.0 ± 0.86, as presented in Figure 5. Figure 6 showcases vital maps that confirms gamma-ray emission from EUVE J0317 - 855: (a) the observed counts map, (b) the model-predicted counts map, (c) the counts residual map reflecting disparities between observed

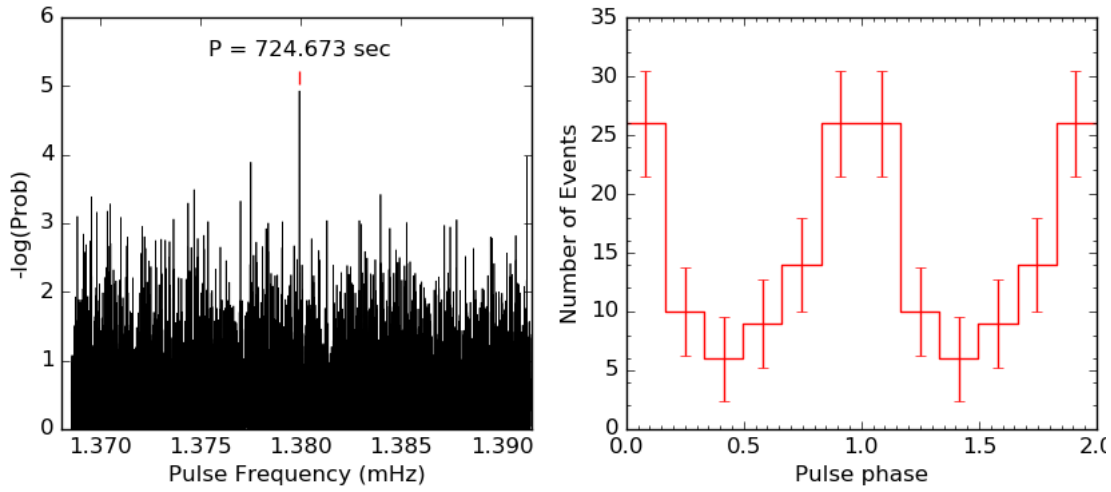

Figure 3: Left: The power spectrum produced using the Rayleigh test display a pulsed modulation at the spin period of the white dwarf with a chance probability that it could be associated with noise of $P \sim 1.5 \times 10^{-5}$, rejecting the null-hypothesis of no significant emission at the spin period of the white dwarfs at the 99.9984% level. Right: gamma-ray phase light curve of J0317 in the energy range 1.3-10 GeV, with photons extracted from a ROI with radius of 0.6° folded with Ferrario et al. [25] ephemeris T_0 = 2450237.715035 BJD, with P ≈ 12 mins.

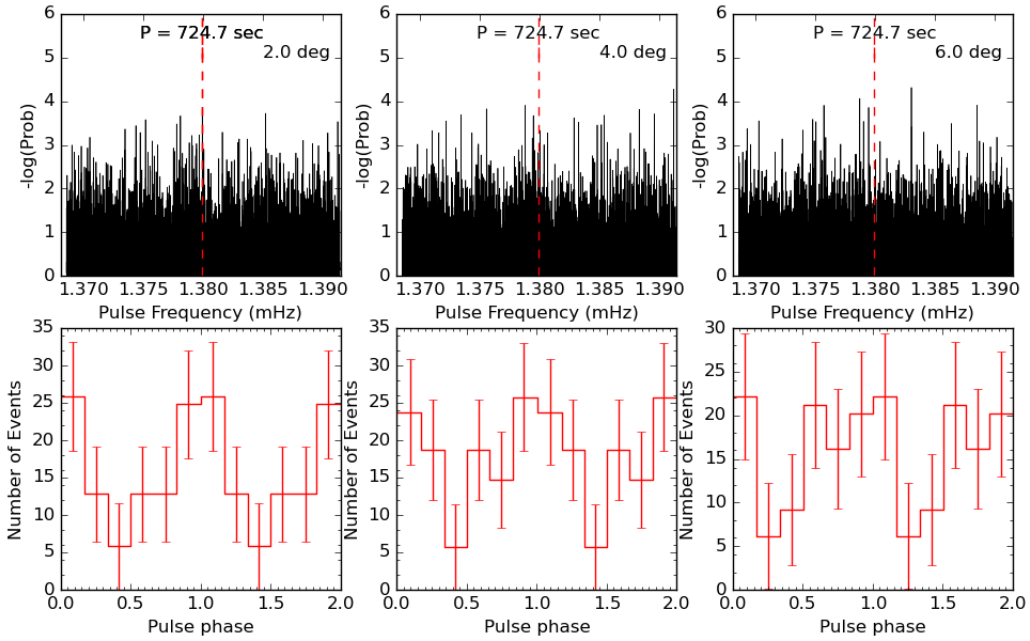

Figure 4: The corresponding power spectra and phase folded light curves in regions of the sky 2° and 4° and 6° away from the source's position in the sky for comparison.

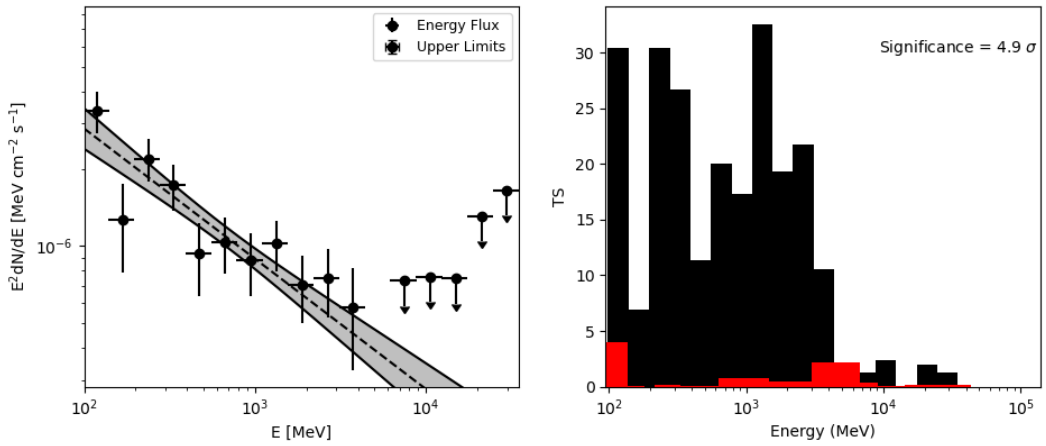

Figure 5: The energy flux spectrum plot of CTCV J2056−3014 over the energy range 0.1−500 GeV for the entire observation period is displayed with a power-law model fitted to the energy flux points with a photon index 2.0 ± 0.86. Left panel: is generated through binned analysis from events selected using TS gating briefly discussed earlier; Right panel: The corresponding significance of the TS-gated (Black) and ungated (noise) data (Red) distributed as a function of energy for each energy bin with measurable signal, which reveals a significance of (4.9 σ) using Equation 1 with the emission mainly restricted to energy bins $\epsilon_\gamma \leq 10$ GeV.

and predicted counts, and where (d) presents the TS residual map, highlighting excess gamma-rays at the location of CTCV J2056−3014. These maps collectively assess the model's accuracy e.g., by comparing observed and predicted counts. We searched for periodic oscillations in the energy range with energy maximum set at 10 GeV for photon events within 0.6° ROI. We folded the 29.6 s period [26] on an arbitrary reference time due to the absence of a published ephemeris. The offset was subtracted to center the pulse on this arbitrary reference time (BJD = 2457463.32751380) . The phased light curve and the Rayleigh test power spectrum are presented in Figure 7.

From Figure 8 it is evident that the pulsations lost its coherence in the off-source regions which seems to suggest that the pulsations also correspond mainly to the position of CTCV J2056 in the sky.

4.3 LAMOST J024048.51+195226.9

LAMOST J024048.51+195226.9 was detected with a significance level 5.4 σ, and it exhibited a predicted count of 1700 with an energy flux of ($8.66 \times 10^{-6} \pm 6.74 \times 10^{-7}$ MeV cm^{-2} s^{-1}). The Fermi-LAT energy flux spectrum of LAMOST J024048.51+195226.9 displays a spectrum that can be fitted with a power-law model with an index of 1.9 ± 0.87, as presented in Figure 9. Figure 10 showcases vital maps that confirms gamma-ray emission from LAMOST J024048.51+195226.9: (a) the observed counts map, (b) the model-predicted counts map, (c) the counts residual map reflecting disparities between observed and predicted counts, and where (d) presents the TS residual map, highlighting excess gamma-rays at the location of LAMOST J024048.51+195226.9. These maps collectively assess the model's accuracy e.g., by comparing observed and predicted counts. We searched for periodic oscillations in the energy range with energy maximum set at 10 GeV using photons events within 0.6° ROI using the ephemeris calculated by Pelisoli et al [32] (T_0 =

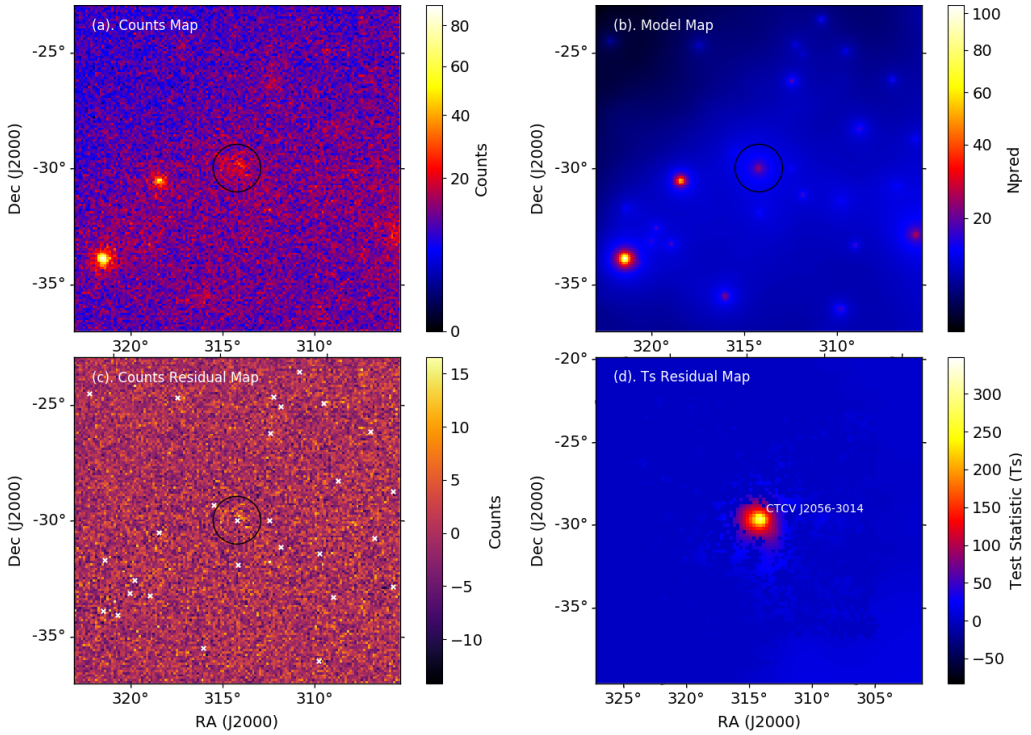

Figure 6: (a) Observed counts map, (b) model predicted counts, (c) the counts residual map. All significant sources included in the model will show with their predicted counts (Npred). The residual map displays the goodness of the model. If there is a huge difference between predicted counts and observed counts the effect will be seen as extreme negative or positive counts at the location where counts are overestimated or underestimated. (d) TS residual map shows excess γ-rays above the background at the location of CTCV J2056−3014 at the 4.9 σ level when the model predictions for the rest of the sources in the field have been removed.

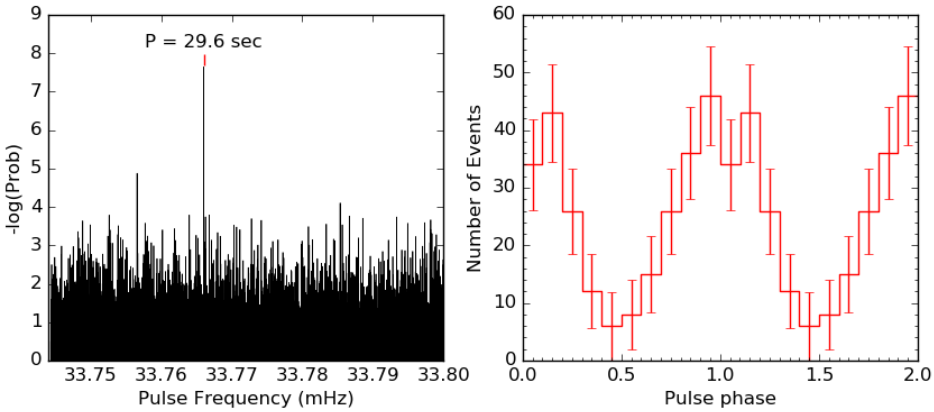

Figure 7: Left: The power spectrum produced using the Rayleigh test display a clear spike at the spin period of the white dwarf in J2056 at a probability that it is due to chance $P = 3.1 \times 10^{-8}$ rejecting the hypothesis of no pulsed emission at the spin-period of the white dwarf at the 99.9999968%. Right: gamma-ray phase light curve of J2056 in the energy range 0.9-10 GeV, with photons extracted from a ROI with radius of 0.6° folded at 29.6 seconds [26] with an arbitrary reference time.

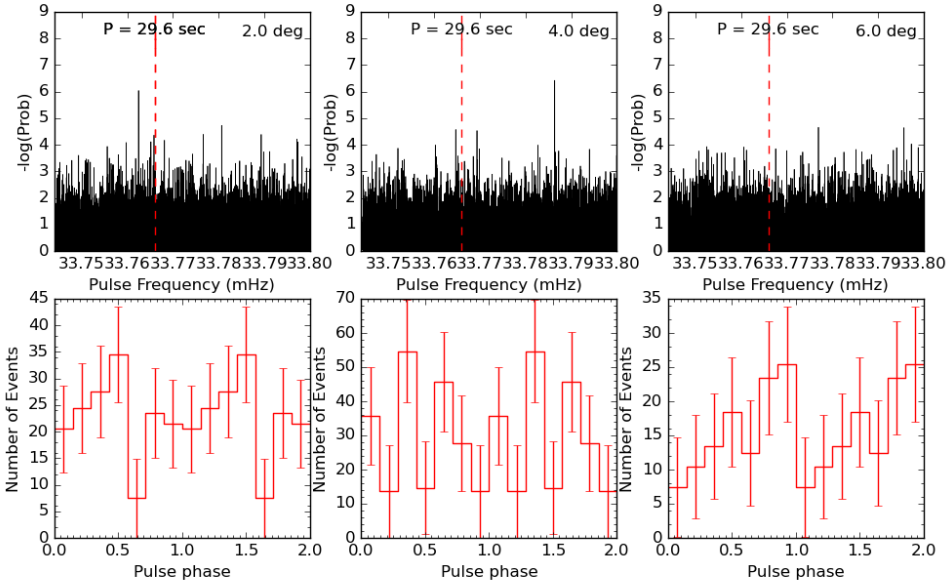

Figure 8: The corresponding power spectrum and phase folded light curves in regions of the sky 2° and 4° and 6° away from the source's position in the sky for comparison.

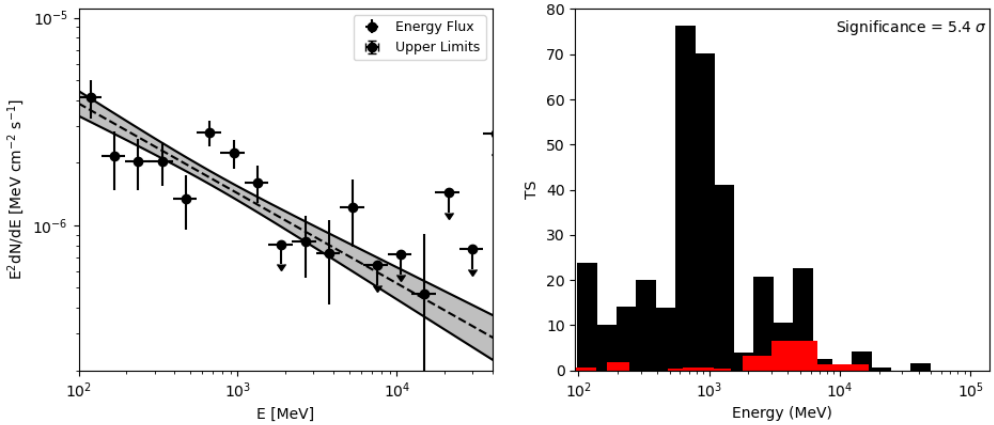

Figure 9: The energy flux spectrum plot of LAMOST J024048.51+195226.9 over the energy range 0.1−500 GeV for the entire observation period is displayed with a power-law model fitted to the energy flux points with a photon index 1.9 ± 0.87. Left panel: is generated through binned analysis from events selected using TS-gating briefly discussed earlier; Right panel: The corresponding significance of the TS-gated (Black) and ungated (noise) data (Red) distributed as a function of energy for each energy bin with measurable signal, which reveals a significance of (5.4 σ) using Equation 1 with the emission mainly restricted to the energy bins $\epsilon_\gamma \leq 10$ GeV.

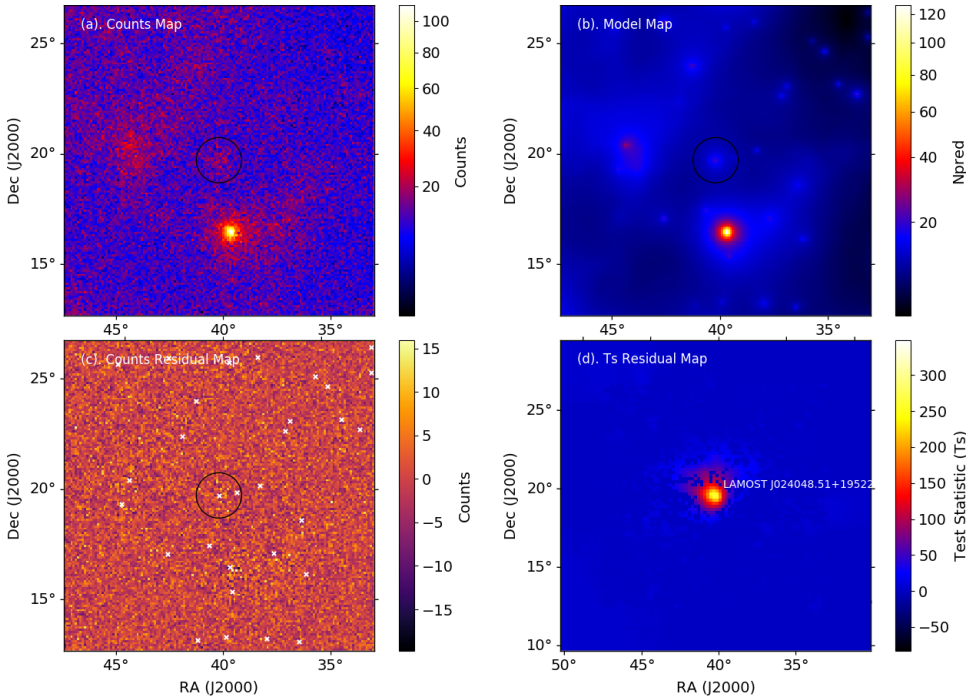

Figure 10: (a) Observed counts map, (b) model predicted counts map, (c) counts residual map. All significant sources included in the model will show with their predicted counts (Npred). The residual map displays the goodness of the model. If there is a huge difference between predicted counts and observed counts the effect will be seen as extreme negative or positive counts at the location where counts are overestimated or underestimated. (d) TS residual map shows excess γ-rays above the background at the location of LAMOST J024048.51 + 195226.9 at the 5.4 σ significance level when the models predictions for the rest of the sources in the field have been removed.

2459434.6780256, where time of pulse-maximum T_0 is expressed in BJD). The phased light curve and the Rayleigh test power spectrum are presented in Figure 11.The off-source control analysis displayed in Figure 12 suggests that the 29.93 pulsations seems to come mainly from the position of LAMOST J024048.51+19522.6 in the sky.

5. Discussion and Conclusion

The objective of this study was to utilize Fermi LAT gamma ray data to search for steady and pulsed gamma-ray emissions from magnetized white dwarfs with short rotational periods and/or strong magnetic fields which are not directly accreting matter from a companion star. The primary goal was to investigate the possibility of these sources as potential emitters of gamma rays. The results presented in this study are based on a preliminary analysis of sample sources, including EUVE J0317-855, CTCV J2056-3014, and LAMOST J024048.51+195226.9. Our analysis is based upon optimizing a weak but persistent gamma-ray presence by flagging data where good model convergence is obtained. Our results seem to support theoretical model predictions [9] that gamma-ray emission is restricted to energies $\epsilon_\gamma \leq 10\,\mathrm{GeV}$, at the $\sim 5\sigma$ significance level for all three sources. The search for possible periodicity of gamma-ray emissions from these sources

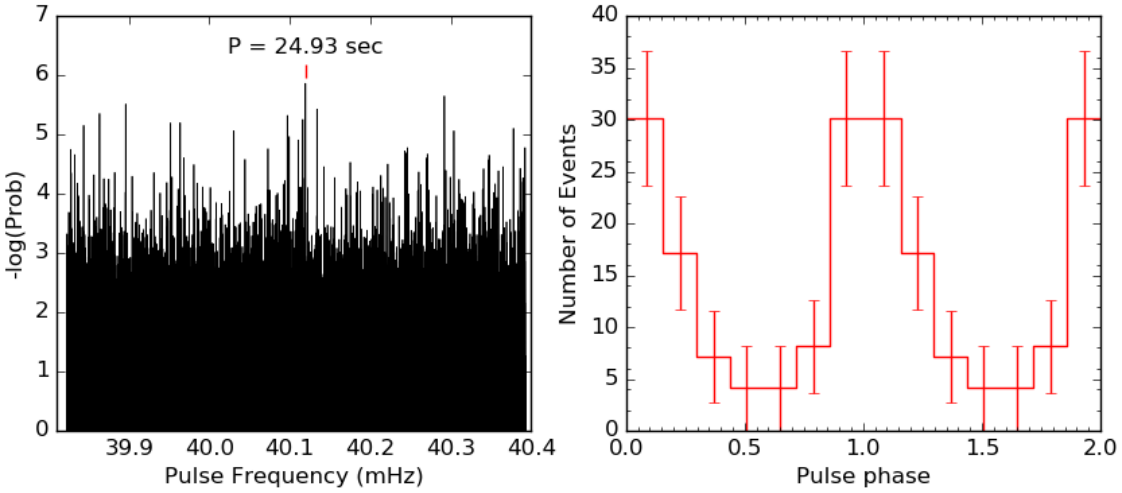

Figure 11: Left: The power spectrum produced using the Rayleigh test display a clear spike at the spin period of the white dwarf in J0240 with a probability that it may be due to chance of $P \sim 1.6 \times 10^{-6}$ rejecting the null-hypothesis of no pulsed emission at he spin period of the white dwarf at the 99.99984%. Right: gamma-ray phase light curve of J0240 in the energy range 1.5-10 GeV, with photons extracted from a ROI with radius of 0.6° folded with Pelisoli et al [32] ephemeris (epoch of the first maximum T_0 = 2459434.6780256 BJD, and P ≈ 24.9 seconds).

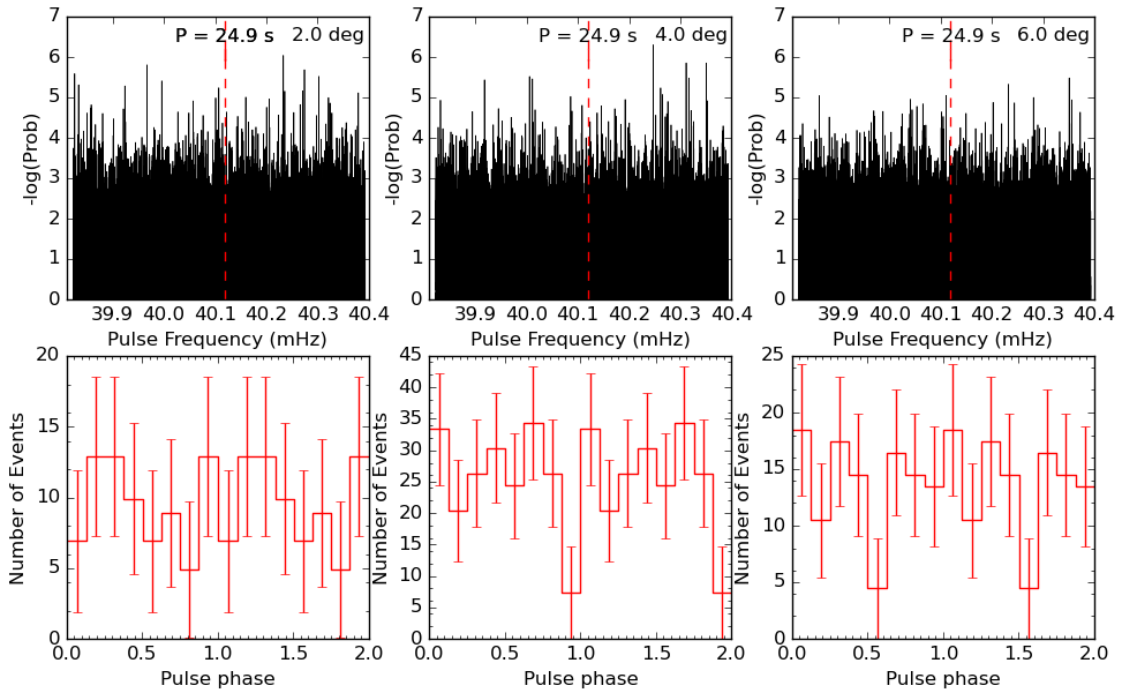

Figure 12: The corresponding power spectrum and phase folded light curves in regions of the sky 2° and 4° and 6° away from the source's position in the sky for comparison.

revealed the detection of pulsed gamma-rays at the rotational period of these white dwarfs. Our control analyses in off-source regions 2°, 4° and 6° away from the source's position in the sky seem to suggest that the periodic emission is mainly restricted to the position of the source in the sky.

These findings suggest that magnetized white dwarfs may be candidates for low-level gamma-ray emission. Thus, follow up studies using MeerKAT need to be performed to assess whether the these sources are consistent non-thermal emitters through some pulsar-like process. This had been done for AE Aquarii and AR Scorpii, which showed pulsar-like radio L-band emission which complemented the pulsed emission seen in the Fermi-LAT data [47]. Further studies could help to clarify the nature of the gamma-ray emissions from these white dwarfs and to determine the extent to which it occurs. These insights could deepen our understanding of the mechanisms behind the multi-wavelength emission of white dwarfs.

Acknowledgments

The authors thank a reviewer for very constructive feed-back which improved the paper.

References

[1] B. W. Carroll and D. A. Ostlie, *An introduction to modern astrophysics and cosmology*, *An introduction to modern astrophysics and cosmology/BW Carroll and DA Ostlie. 2nd edition. San Francisco: Pearson* (2006) .

[2] K. B. Burdge, T. A. Prince, J. Fuller, D. L. Kaplan, T. R. Marsh, P.-E. Tremblay et al., *A systematic search of zwicky transient facility data for ultracompact binary lisa-detectable gravitational-wave sources*, *The Astrophysical Journal* **905** (2020) 32.

[3] W. R. Brown, M. Kilic, A. Kosakowski, J. J. Andrews, C. O. Heinke, M. A. Agüeros et al., *The elm survey. viii. ninety-eight double white dwarf binaries*, *The Astrophysical Journal* **889** (2020) 49.

[4] K. J. Shen, *Every interacting double white dwarf binary may merge*, *The Astrophysical Journal Letters* **805** (2015) L6.

[5] I. Caiazzo, K. B. Burdge, J. Fuller, J. Heyl, S. Kulkarni, T. A. Prince et al., *A highly magnetized and rapidly rotating white dwarf as small as the moon*, *Nature* **595** (2021) 39.

[6] C. A. Tout, D. Wickramasinghe, J. Liebert, L. Ferrario and J. Pringle, *Binary star origin of high field magnetic white dwarfs*, *Monthly Notices of the Royal Astronomical Society* **387** (2008) 897.

[7] E. García-Berro, P. Lorén-Aguilar, G. Aznar-Siguán, S. Torres, J. Camacho, L. G. Althaus et al., *Double degenerate mergers as progenitors of high-field magnetic white dwarfs*, *The Astrophysical Journal* **749** (2012) 25.

[8] J. Schwab, *Evolutionary models for the remnant of the merger of two carbon-oxygen core white dwarfs*, *The Astrophysical Journal* **906** (2021) 53.

[9] P. J. Meintjes, S. T. Madzime, Q. Kaplan and H. J. van Heerden, *Spun-up rotation-powered magnetized white dwarfs in close binaries as possible gamma-ray sources: Signatures of pulsed modulation from ae aquarii and ar scorpii in fermi-lat data*, *Galaxies* **11** (2023) 14.

[10] V. Usov, *Generation of gamma-rays by a rotating magnetic white dwarf*, *Soviet Astronomy Letters* **14** (1988) 258.

[11] K. Kashiyama, K. Ioka and N. Kawanaka, *White dwarf pulsars as possible cosmic ray electron-positron factories*, *Physical Review D* **83** (2011) 023002.

[12] V. Usov, *High-frequency emission of x-ray pulsar 1e 2259+ 586*, *Astrophysical Journal, Part 1 (ISSN 0004-637X), vol. 410, no. 2, p. 761-763.* **410** (1993) 761.

[13] R. V. Lobato, J. Coelho and M. Malheiro, *Radio pulsar death lines to sgrs/axps and white dwarfs pulsars*, in *AIP Conference Proceedings*, vol. 1693, p. 030003, AIP Publishing LLC, 2015.

[14] R. Lobato, J. Coelho and M. Malheiro, *Particle acceleration and radio emission for sgrs/axps as white dwarf pulsars*, in *Journal of Physics: Conference Series*, vol. 630, p. 012015, IOP Publishing, 2015.

[15] R. V. Lobato, J. G. Coelho and M. Malheiro, *Ultra-high energy cosmic rays from white dwarf pulsars and the hillas criterion*, in *Journal of Physics: Conference Series*, vol. 861, p. 012005, IOP Publishing, 2017.

[16] S. Mereghetti, *The strongest cosmic magnets: soft gamma-ray repeaters and anomalous x-ray pulsars*, *The Astronomy and Astrophysics Review* **15** (2008) 225.

[17] V. M. Kaspi, *Soft gamma repeaters and anomalous x-ray pulsars: Together forever*, in *Symposium-International Astronomical Union*, vol. 218, pp. 231–238, Cambridge University Press, 2004.

[18] M. Malheiro, J. A. Rueda and R. Ruffini, *Sgrs and axps as rotation-powered massive white dwarfs*, *Publications of the Astronomical Society of Japan* **64** (2012) .

[19] J. Coelho and M. Malheiro, *Similarities of sgrs with low magnetic field and white dwarf pulsars*, in *International Journal of Modern Physics: Conference Series*, vol. 18, pp. 96–100, World Scientific, 2012.

[20] S. T. Madzime, P. Meintjes, K. K. Singh and H. van Heerden, *Search for gamma-ray emission from the nova-like variable AE Aquarii using the Fermi-LAT Pass 8 data Archive*, in *Proceedings of 7th Annual Conference on High Energy Astrophysics in Southern Africa — PoS(HEASA2019)*, vol. 371, p. 051, 2020, DOI.

[21] S. Madzime, P. Meintjes, H. van Heerden, K. Singh, D. Buckley, P. Woudt et al., *The detection of pulsed emission at the spin-period of the white dwarf in ae aquarii in meerkat and fermi-lat data*, in *Proceedings of the 8th High Energy Astrophysics in Southern Africa (HEASA2021) Conference, Online*, pp. 13–17, 2021.

[22] S. T. Madzime, *The search for pulsed radio and gamma-ray emission from the cataclysmic variable system ae aquarii using meerkat and fermi-lat data*, Master's thesis, University of the Free State, 2021.

[23] Q. Kaplan, P. Meintjes and H. van Heerden, *Low-power pulsed emission at the spin period of the white dwarf in ar scorpii?*, .

[24] M. Barstow, S. Jordan, D. O'Donoghue, M. Burleigh, R. Napiwotzki and M. Harrop-Allin, *Re j0317–853: the hottest known highly magnetic da white dwarf*, *Monthly Notices of the Royal Astronomical Society* **277** (1995) 971.

[25] L. Ferrario, S. Vennes, D. Wickramasinghe, J. Bailey and D. Christian, *Euve j0317—855: a rapidly rotating, high-field magnetic white dwarf*, *Monthly Notices of the Royal Astronomical Society* **292** (1997) 205.

[26] R. L. de Oliveira, A. Bruch, C. Rodrigues, A. Oliveira and K. Mukai, *Ctcv j2056-3014: An x-ray-faint intermediate polar harboring an extremely fast-spinning white dwarf*, *The Astrophysical Journal Letters* **898** (2020) L40.

[27] T. Augusteijn, C. Tappert, T. Dall and J. Maza, *Cataclysmic variables from the calán–tololo survey–ii. spectroscopic periods*, *Monthly Notices of the Royal Astronomical Society* **405** (2010) 621.

[28] C. Bailer-Jones, J. Rybizki, M. Fouesneau, G. Mantelet and R. Andrae, *Estimating distance from parallaxes. iv. distances to 1.33 billion stars in gaia data release 2*, *The Astronomical Journal* **156** (2018) 58.

[29] C. B. Haakonsen and R. E. Rutledge, *Xid ii: Statistical cross-association of rosat bright source catalog x-ray sources with 2mass point source catalog near-infrared sources*, *The Astrophysical Journal Supplement Series* **184** (2009) 138.

[30] A. Oliveira, C. Rodrigues, D. Cieslinski, F. Jablonski, K. Silva, L. Almeida et al., *Exploratory spectroscopy of magnetic cataclysmic variables candidates and other variable objects*, *The Astronomical Journal* **153** (2017) 144.

[31] W. Hou, A.-l. Luo, Y.-B. Li and L. Qin, *Spectroscopically identified cataclysmic variables from the lamost survey. i. the sample*, *The Astronomical Journal* **159** (2020) 43.

[32] I. Pelisoli, T. Marsh, V. Dhillon, E. Breedt, A. Brown, M. Dyer et al., *Found: a rapidly spinning white dwarf in lamost j024048. 51+ 195226.9*, *Monthly Notices of the Royal Astronomical Society: Letters* **509** (2022) L31.

[33] A. Drake, M. Graham, S. Djorgovski, M. Catelan, A. Mahabal, G. Torrealba et al., *The catalina surveys periodic variable star catalog*, *The Astrophysical Journal Supplement Series* **213** (2014) 9.

[34] C. Littlefield and P. Garnavich, *Identification of orbital eclipses in lamost j024048. 51+ 195226.9, a candidate ae aqr-type cataclysmic variable star*, *Research Notes of the AAS* **4** (2020) 171.

[35] P. Garnavich, C. Littlefield, R. Wagner, J. Van Roestel, A. D. Jaodand, P. Szkody et al., *Confirmation of a second propeller: A high-inclination twin of ae aquarii*, *The Astrophysical Journal* **917** (2021) 22.

[36] J. R. Thorstensen, *Follow-up studies of five cataclysmic variable candidates discovered by lamost*, *The Astronomical Journal* **160** (2020) 151.

[37] G. A. Wynn, A. R. King and K. Horne, *A magnetic propeller in the cataclysmic variable ae aquarii*, *Monthly Notices of the Royal Astronomical Society* **286** (1997) 436.

[38] M. Pretorius, D. Hewitt, P. Woudt, R. Fender, I. Heywood, C. Knigge et al., *Radio and optical observations of the possible ae aqr twin, lamost j024048. 51+ 195226.9*, *Monthly Notices of the Royal Astronomical Society* **503** (2021) 3692.

[39] W. Atwood, A. A. Abdo, M. Ackermann, W. Althouse, B. Anderson, M. Axelsson et al., *The large area telescope on the fermi gamma-ray space telescope mission*, *The Astrophysical Journal* **697** (2009) 1071.

[40] W. Atwood, A. Albert, L. Baldini, M. Tinivella, J. Bregeon, M. Pesce-Rollins et al., *Pass 8: toward the full realization of the fermi-lat scientific potential*, *arXiv preprint arXiv:1303.3514* (2013) .

[41] J. R. Mattox, D. Bertsch, J. Chiang, B. Dingus, S. Digel, J. Esposito et al., *The likelihood analysis of egret data*, *The Astrophysical Journal* **461** (1996) 396.

[42] M. Arakawa, M. Hayashida, D. Khangulyan and Y. Uchiyama, *Detection of small flares from the crab nebula with fermi-lat*, *The Astrophysical Journal* **897** (2020) 33.

[43] S. Abdollahi, F. Acero, M. Ackermann, M. Ajello, W. Atwood, M. Axelsson et al., *Fermi large area telescope fourth source catalog*, *The Astrophysical Journal Supplement Series* **247** (2020) 33.

[44] O. De Jager, B. Raubenheimer and J. Swanepoel, *A poweful test for weak periodic signals with unknown light curve shape in sparse data*, *Astronomy and Astrophysics* **221** (1989) 180.

[45] P. S. Ray, M. Kerr, D. Parent, A. Abdo, L. Guillemot, S. Ransom et al., *Precise γ-ray timing and radio observations of 17 fermi γ-ray pulsars*, *The Astrophysical Journal Supplement Series* **194** (2011) 17.

[46] G. Hobbs, R. Edwards and R. Manchester, *Tempo2, a new pulsar-timing package–i. an overview*, *Monthly Notices of the Royal Astronomical Society* **369** (2006) 655.

[47] P. Meintjes, S. Madzime, Q. Kaplan, H. van Heerden, K. Singh, D. Buckley et al., *Particle acceleration and high energy emission in the white dwarf binaries ae aquarii and ar scorpii*, in *The Sixteenth Marcel Grossmann Meeting on Recent Developments in Theoretical and Experimental General Relativity, Astrophysics and Relativistic Field Theories: Proceedings of the MG16 Meeting on General Relativity Online; 5–10 July 2021*, pp. 4522–4531, World Scientific, 2023.